echanical Engineering is defined nowadays as a discipline hich involves the application of principles of physics, sign, manufacturing and maintenance of mechanical stems". Recently, mechanical engineering has also cused on some cutting-edge subjects such as nomechanics and nanotechnology, mechatronics and botics, computational mechanics, biomechanics, ernative energies, as well as aspects related to stainable mechanical engineering.

is book covers mechanical engineering higher education th a particular emphasis on quality assurance and the provement of academic institutions, mechatronics ucation and the transfer of knowledge between university d industry.

Paulo Davim is Aggregate Professor in the Department Mechanical Engineering at the University of Aveiro, rtugal and is Head of MACTRIB (Machining and Tribology search Group). His main research interests include anufacturing, materials and mechanical engineering.

WILEY

Edited by
J. Paulo Davim

Mechanical Engineering Education

WILEY

MECHANICAL ENGINEERING AND SOLID MECHANICS SERIES

Mechanical Engineering Education

Edited by
J. Paulo Davim

Chapter 4

Knowledge Transfer between University and Industry: Development of a Vision Measuring System

This chapter discusses the transfer of knowledge between university and industry, and has the potential to benefit both partners, in designing innovative solutions, in the optimal allocation of resources, in motivating the students for new challenging tasks and finally in integrating multidisciplinary University/Industry teams.

The case study presented here is related to the field of industrial maintenance, concerning the measuring and monitoring of the railroad wheel profiles by the Portuguese railway company, Comboios Portugal (CP).

A vision system to measure the wearing of the wheels of a train moving at a slow speed of 5 km/h is studied here. A 1:1 scale static prototype is developed and the calibration and testing procedures are presented.

Chapter written by João M.G. FIGUEIREDO.

The developed prototype is based on an image processing system to provide for the automatic measurement of the moving wheels. The wheel's profile is acquired by the illumination of the wheel through a secant horizontal light plane. The profile's image is processed by identifying the line of the greatest light gradient in the whole image. The gradient's profile is then converted to the wheel's radial profile by means of a coordinate transformation model, which transforms the image plane into the wheel's radial plane.

Experimental results are presented and discussed in the following sections.

4.1. Introduction

Metrology is mainly concerned with the study of measuring instruments or methods and the treatment of the measurement results. The research and development of new measurement devices and procedures conducive to smaller uncertainties is a permanent challenge to the innovative skills of the metrologist.

The measurement of the railroad wheel's profile is a basic procedure in the regular maintenance of trains.

Railroad wheels have to be inspected over regular time intervals to evaluate the wearing out of the rolling surface. Wheels that have excessive wearing face a very high risk of jumping off the rails, causing a serious train accident.

Depending on the physical characteristics of the railroad and on the train's average velocity, there are different wearing profiles. Each wearing profile characterizes the correspondent railroad line. The physical factors such as the train velocity, the amplitude of the railroad curves, the number of curves to the left and to the right and so on

influence the wearing of the wheel's profile. Figure 4.1 shows a standard profile and a wasted profile of a wheel.

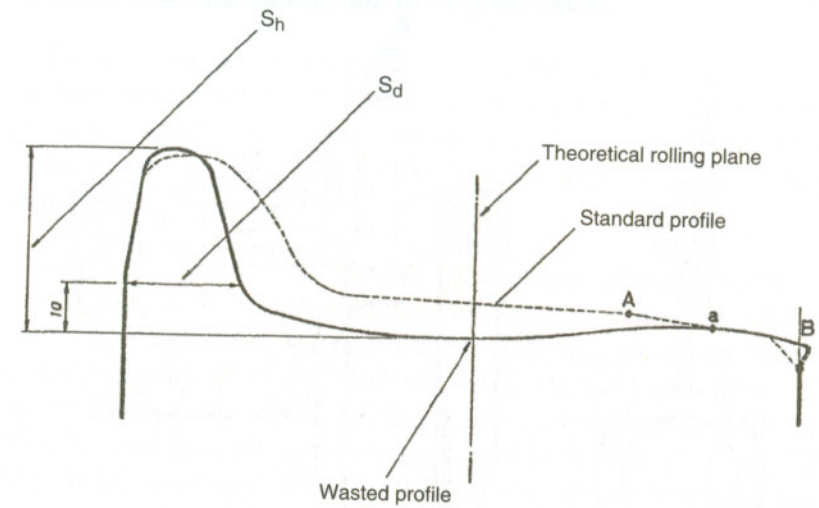

Figure 4.1. *Standard and wasted wheel's profile*

Manual measuring devices based on the well-known sliding caliper are the usual methods to evaluate the profile's dimensional characteristics, as shown in Figure 4.2.

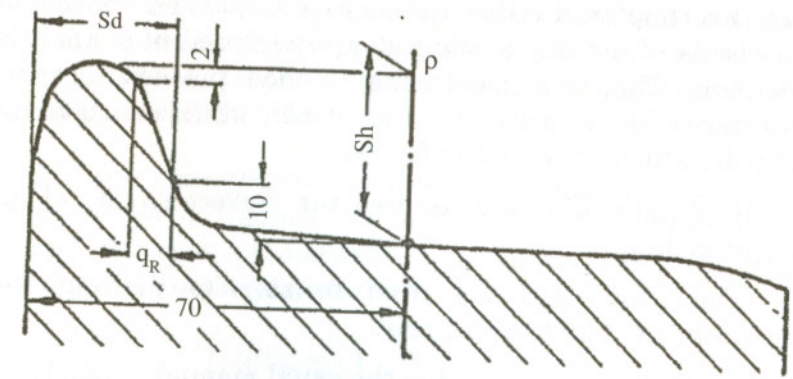

Figure 4.2. *Controlled dimensions of a wheel's profile*

Figure 4.3 shows a usual mechanical measuring device used in the Portuguese national railways company.

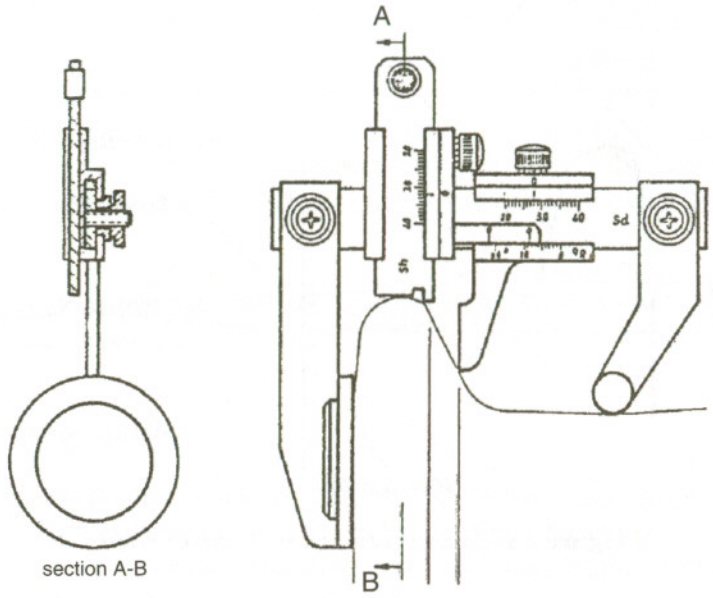

Figure 4.3. *Standard mechanical measuring device to measure the wheel's profile*

In this chapter, a vision system to measure the wearing of the wheels of a train moving at a slow speed of 5 km/h is developed. This new measuring method presents several advantages in relation to the usual standard manual methods, which are listed as follows:

– It is automatic and assures the correct saving of all measured data.

– The train does not need to stop to perform the measurement of all train wheels.

– It is very fast compared to the usual manual methods.

– It evaluates not only a few controlled dimensions of the profile but also the total profile.

Image processing technology is a very interesting solution in industry environments when a quick, accurate and traceable measurement has to be performed.

Image processing measurement systems are very useful in the manufacturing industry of components, verifying physical attributes (dimensions, color, etc.), the relative position of parts in subassembly sets, manufacturer labels and so on.

Artificial vision and image processing already have an important role in several technological domains as (1) pattern recognition, with multiple applications in industrial quality control [DU 08, GRI 08, KIM 10, ZHA 10, ZHA 12], medical diagnosis [GOU 07, BRO 10], face detection [GRI 09, PAI 10] and geometry restoration [HLO 03, LIM 11, CHE 12]; (2) visual servoing [NEL 03]; and (3) object tracking and movement detection [ALE 98, LEE 06, GRI 07, CUI 08, MES 10, YAN 10].

Among the different movement detection methods, there are two main processing methods: *interframe differencing* and *reference frame differencing*. The performance of both methods is drastically influenced by the pixel area where the method is applied and the subsequent use of the obtained results. These processing results are usually used in real-time monitoring [FAT 95] and video compression applications [JAI 81, MIT 96].

In the *interframe differencing method* [JAI 95], performance is defined for each pixel (x, y) between the frame obtained at instant t_1 (t_1-frame) and the frame obtained at instant t_2 (t_2-frame):

$$Dp(x, y) = \begin{cases} 1, \left|F(x, y, t_1) - F(x, y, t_2)\right| \geq \tau \\ 0, \text{otherwise} \end{cases} \quad [4.1]$$

where $Dp(x, y)$ is the difference in the intensity level of the pixel (x, y) and τ represents the threshold in the number of different pixels.

In the *reference frame differencing method* [JAI 95], performance is defined for each pixel (x, y) between the reference frame F_r and the t_n frame:

$$Dp(x, y) = \begin{cases} 1, \left|F_r(x, y, t_r) - F(x, y, t_n)\right| \geq \tau \\ 0, \text{otherwise} \end{cases} \quad [4.2]$$

where t_r and t_n represent the instants where the frames F_r and F_n were acquired, respectively.

The vision system to measure the wearing of a train's wheel moving at a slow speed of 5 km/h is studied through the development of a static 1:1 scale prototype in which calibration and testing procedures are presented. The developed prototype is based on an image processing system to provide for the automatic measurement of moving railroad wheels. The wheel's profile is acquired by the illumination of the wheel through a secant and horizontal light plane. This profile's image is processed by identifying the line of the greatest light gradient in the whole image. This gradient profile is then converted into the wheel radial profile by means of a coordinate transformation model, which transforms the image plane into the wheel's radial plane.

4.2. Measuring system

The developed measuring system comprises the following parts:

– light plane secant to the wheel;

– vision system (camera and image processing system);

– sensors to activate or deactivate the vision system;

– operator panel to display the results.

Figure 4.4 shows the system concept with the integration of all major components.

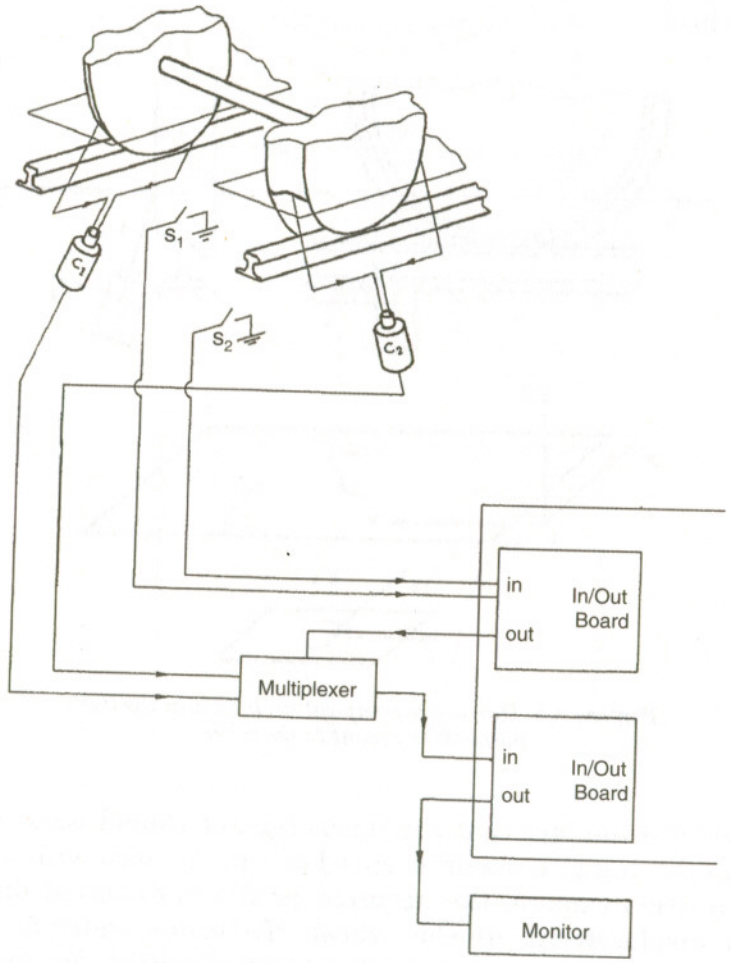

Figure 4.4. *System concept*

4.2.1. *Light plane*

The proper identification of the wheel's profile in the captured image is very important for an accurate measurement. Figure 4.5 illustrates the schematic hardware implementation to obtain the projected light plane, secant to the wheel.

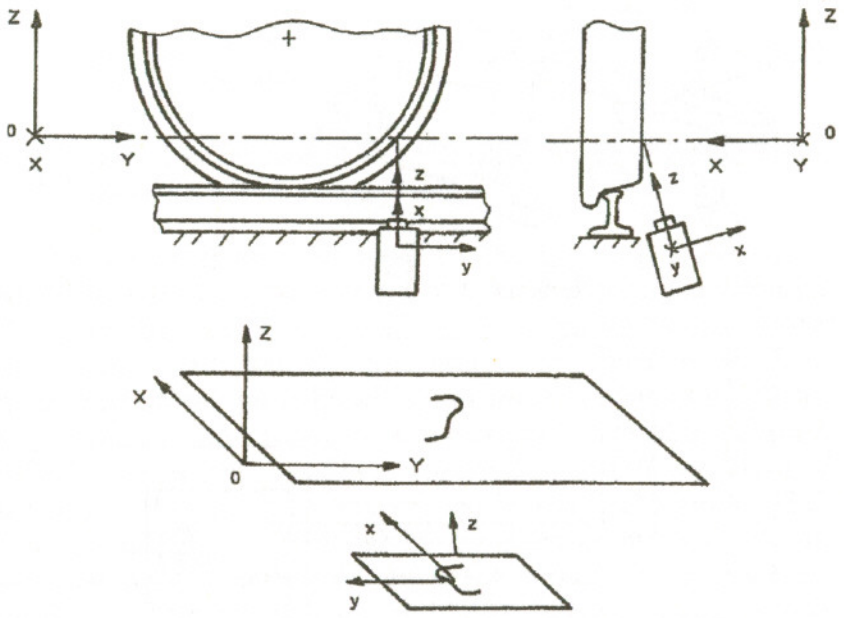

Figure 4.5. *Hardware composition to obtain the light plane XOY secant to the wheel*

Due to the fact that the measurement should occur on a train moving at a maximal speed of 5 km/h, even with a fast acquisition camera, the acquired profile is distorted due to the displacement of the wheel. To compensate for the previously mentioned distortion, a dual profile acquisition system was implemented through a mirror's composition, to maintain the line distance between two relative light profiles. Figure 4.6 illustrates the implemented system.

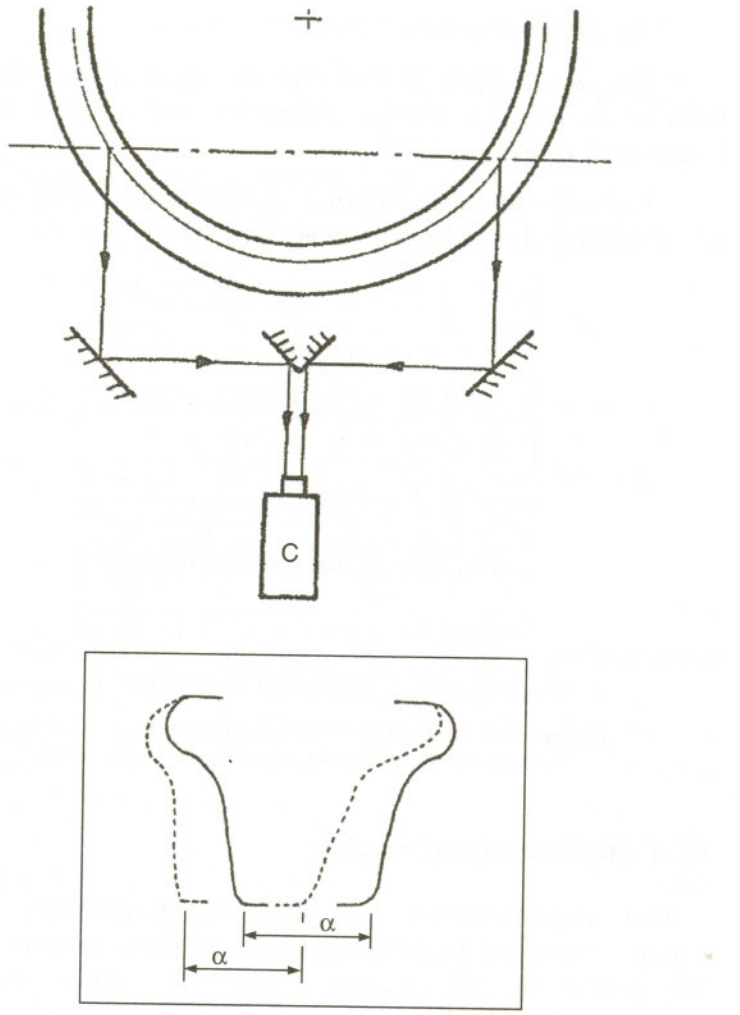

Figure 4.6. *Dual profile at image plane*

Figure 4.7 illustrates the distortion of a wheel's profile caused by the image acquisition of a moving wheel.

The advantages of the dual system are as follows:

– Two light profiles are acquired with only one video camera.

– The processing time is reduced by half.

– The knowledge of the two image profiles allows the calculation of the rolling diameter (as it will be later illustrated in Figure 4.13).

– Two corresponding points in the same image diameter are obtained almost simultaneously.

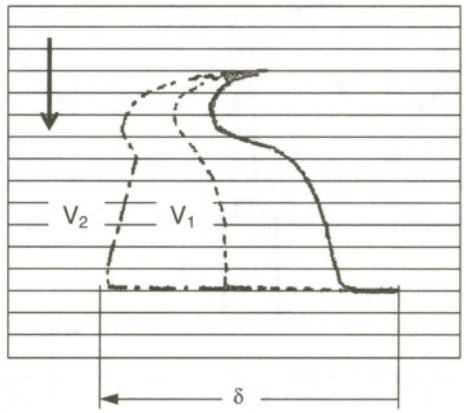

Figure 4.7. *Distortion of the wheel's profile caused by a moving wheel with velocities V_1 and V_2 ($V_1 < V_2$)*

4.2.2. *Mathematical model*

The measurement of physical dimensions through image processing techniques must, at first, be able to relate 3D points to 2D images [GON 87]. This perspective transformation is illustrated in Figure 4.8, and it can be implemented as stated in equation [4.3].

$$\begin{bmatrix} c_{h1} \\ c_{h2} \\ c_{h3} \\ c_{h4} \end{bmatrix} = \begin{bmatrix} 1 & 0 & 0 & 0 \\ 0 & 1 & 0 & 0 \\ 0 & 0 & 1 & 0 \\ 0 & 0 & -1/\lambda & 1 \end{bmatrix} \cdot \begin{bmatrix} x \\ y \\ z \\ 1 \end{bmatrix} \qquad [4.3]$$

where:

(c_{h1}, c_{h2}, c_{h3}, c_{h4}) are homogeneous coordinates in the image plane;

(X, Y, Z) are space coordinates; and

λ is the camera focal distance.

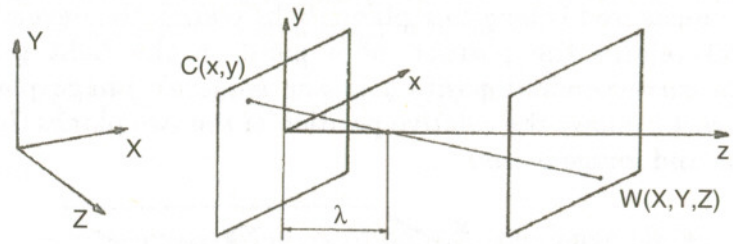

Figure 4.8. *Perspective transformation*

The relationship between the image homogeneous coordinates and the image Cartesian coordinates are

$$[x] = \left[c_{h1} / c_{h4} \right] \qquad [4.4]$$

$$[y] = \left[c_{h2} / c_{h4} \right] \qquad [4.5]$$

$$[z] = \left[c_{h3} / c_{h4} \right] \qquad [4.6]$$

Substituting the above equations, we obtain the image Cartesian coordinates (x, y):

$$\begin{bmatrix} x \\ y \end{bmatrix} = \begin{bmatrix} \dfrac{\lambda X}{\lambda - Z} \\ \dfrac{\lambda Y}{\lambda - Z} \end{bmatrix} \qquad [4.7]$$

where:

(x, y) are coordinates in the image plane;

(X, Y, Z) are space coordinates;

λ is the camera focal distance.

In the case studied in this chapter, as the physical points to be measured belong to a plane (light plane), the developed model relates the position of a point in the light plane to its correspondent position in the camera's image plane. Figure 4.9 shows the relative position of the two planes (light plane and image plane).

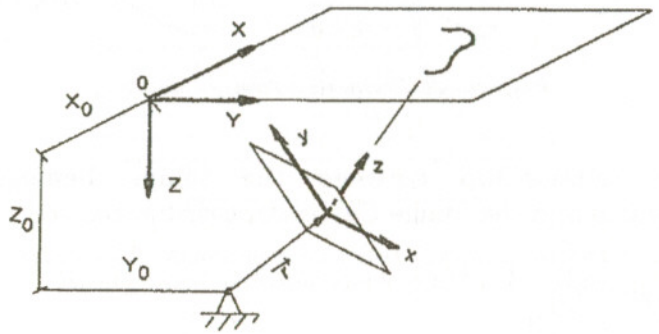

Figure 4.9. *Relative position of the light plane and the image plane*

A transformation model is needed to relate the two planes. This transformation can be implemented considering six degrees of freedom: three displacements (X, Y, Z) and three rotations (α, β, θ). A possible sequence of mathematical transformations applied to the camera's referential to place the image plane coincident to an arbitrary space plane can be obtained by [FIG 08]:

1) displacement of the camera fixation point from the origin to the final point (X_0, Y_0, Z_0) – G;

2) rotation of the x-axis by α degrees – $R(x, \alpha)$;

3) rotation of the y-axis by β degrees – $R(y, \beta)$;

4) rotation of the z-axis by θ degrees – $R(z, \theta)$; and

5) displacement of the image plane from the camera fixation point, $\vec{r}(r_1, r_2, r_3) - S$.

The aforementioned transformation sequence can be implemented using equations [4.8], where the transformation matrices are listed in equations [4.9]–[4.14].

$$C_h = P.S.R(z, \theta).R(y, \beta).R(x, \alpha).G.W_h \qquad [4.8]$$

where:

C_h is an homogeneous coordinate in the image plane;

W_h is an homogeneous coordinate of a space point;

$P, S, R(z, \theta), R(y, \beta), R(x, \alpha), G$ are the transformation matrices.

$$G = \begin{bmatrix} 1 & 0 & 0 & -X_0 \\ 0 & 1 & 0 & -Y_0 \\ 0 & 0 & 1 & -Z_0 \\ 0 & 0 & 0 & 1 \end{bmatrix}. \qquad [4.9]$$

$$R(x,\alpha) = \begin{bmatrix} 1 & 0 & 0 & 0 \\ 0 & \cos\alpha & \sin\alpha & 0 \\ 0 & -\sin\alpha & \cos\alpha & 0 \\ 0 & 0 & 0 & 1 \end{bmatrix} \qquad [4.10]$$

$$R(y,\beta) = \begin{bmatrix} \cos\beta & 0 & -\sin\beta & 0 \\ 0 & 1 & 0 & 0 \\ \sin\beta & 0 & \cos\alpha & 0 \\ 0 & 0 & 0 & 1 \end{bmatrix} \qquad [4.11]$$

$$R(z,\theta) = \begin{bmatrix} \cos\theta & \sin\theta & 0 & 0 \\ -\sin\theta & \cos\theta & 0 & 0 \\ 0 & 0 & 1 & 0 \\ 0 & 0 & 0 & 1 \end{bmatrix} \quad [4.12]$$

$$S = \begin{bmatrix} 1 & 0 & 0 & -r_1 \\ 0 & 1 & 0 & -r_2 \\ 0 & 0 & 1 & -r_3 \\ 0 & 0 & 0 & 1 \end{bmatrix} \quad [4.13]$$

$$P = \begin{bmatrix} 1 & 0 & 0 & 0 \\ 0 & 1 & 0 & 0 \\ 0 & 0 & 1 & 0 \\ 0 & 0 & -1/\lambda & 1 \end{bmatrix} \quad [4.14]$$

According to this transformation sequence, we obtain the explicit model that relates the image plane to an arbitrary light plane located in the space [FIG 08]:

$$x = \lambda \frac{N_1(X-X_0)+N_2(Y-Y_0)+N_3(Z-Z_0)-r_1}{-D_1(X-X_0)+D_2(Y-Y_0)+D_3(Z-Z_0)+r_3+\lambda} \quad [4.15]$$

$$y = \lambda \frac{N_4(X-X_0)+N_5(Y-Y_0)+N_6(Z-Z_0)-r_2}{-D_1(X-X_0)+D_2(Y-Y_0)+D_3(Z-Z_0)+r_3+\lambda} \quad [4.16]$$

where:

$N_1 = \cos\beta \cos\theta$

$N_2 = \sin\alpha \sin\beta \cos\beta + \sin\alpha \sin\theta$

$N_3 = \sin\alpha \sin\theta - \cos\alpha \sin\beta \cos\theta$

$N_4 = \cos\beta \sin\theta$

$N_5 = \cos\alpha \cos\theta - \sin\alpha \sin\beta \sin\theta$

$N_6 = \cos\alpha \sin\beta \sin\theta + \sin\alpha \cos\theta$

$D_1 = \sin\beta$

$D_2 = \sin\alpha \cos\beta$

$D_3 = \cos\alpha \cos\beta$

(X, Y, Z) = spatial location of a point W in the global referential;

(X_0, Y_0, Z_0) = spatial location of the camera fixation point in the global referential;

(x, y) = location of the image point C, corresponding to the spatial point W, in the camera referential.

This model, however, does not solve our problem of reconstruction of the reality from the image knowledge. In fact, this model performs exactly the opposite. From the knowledge of the spatial location of a point $W(X, Y, Z)$, it calculates its correspondent location on the image plane $C(x, y)$, knowing all external parameters (X_0, Y_0, Z_0, α, β, θ, r_1, r_2, r_3, λ).

The reconstruction of the reality implies the inverse solution of equations [4.15] and [4.16], which can be achieved by the following transformation:

$$W_h = G^{-1}.R^{-1}(x,\alpha).R^{-1}(y,\beta).R^{-1}(z,\theta).S^{-1}.P^{-1}.C_h \quad [4.17]$$

The solution of this problem is not unique because there is an infinite number of solutions satisfying both equations [4.15] and [4.16], where all the collinear points with the camera image $C(x1, y1)$ and the camera focus are obtained. Therefore, we have to fix the space coordinate Z to obtain a unique solution. In our case, as we have all the points to measure in the same plane (light plane) this restriction has no negative consequences.

Hence, the inverse solution of equations [4.15] and [4.16] can be obtained for a specified Z, in a closed form, as follows [FIG 08]:

$$X = \frac{Q_1 x + Q_2 y + Q_3}{Q_4 x + Q_5 y + Q_6} \qquad [4.18]$$

$$Y = \frac{Q_7 x + Q_8 y + Q_9}{Q_4 x + Q_5 y + Q_6} \qquad [4.19]$$

where:

$$Q_1 = \cos\beta\ \cos\theta + O_1 P_1$$

$$Q_2 = -\sin\theta\ \cos\beta + O_1 P_2$$

$$Q_3 = O_1 P_3 + O_2$$

$$Q_4 = \frac{P_1}{\lambda}$$

$$Q_5 = \frac{P_2}{\lambda}$$

$$Q_6 = \frac{P_3}{\lambda} + 1$$

$$Q_7 = \sin\theta\ \cos\alpha + \cos\theta \sin\beta \sin\alpha + O_3 P_1$$

$$Q_8 = \cos\theta\ \cos\alpha - \sin\theta \sin\beta \sin\alpha + O_3 P_2$$

$$Q_9 = O_3 P_3 + O_4$$

$$P_1 = \frac{(\sin\theta \sin\alpha - \cos\theta \sin\beta \cos\alpha)}{Z/\lambda - O_5}$$

$$P_2 = \frac{(\cos\theta \sin\alpha + \sin\theta \sin\beta \cos\alpha)}{Z/\lambda - O_5}$$

$$P_3 = \frac{O_6 - Z}{Z/\lambda - O_5}$$

$$O_1 = \left(\frac{r_1}{\lambda}\cos\theta - \frac{r_2}{\lambda}\sin\theta\right)\cos\beta + \left(1 + \frac{r_3}{\lambda}\right)\sin\beta + \frac{X_0}{\lambda}$$

$$O_2 = (r_1\cos\theta - r_2\sin\theta)\cos\beta + \left(\frac{r_1}{\lambda}\cos\theta - \frac{r_2}{\lambda}\sin\theta\right)\sin\beta + X_0$$

$$O_3 = \left(\frac{r_1}{\lambda}\sin\theta + \frac{r_2}{\lambda}\cos\theta\right)\cos\alpha - \left(\left(\frac{r_2}{\lambda}\sin\theta - \frac{r_1}{\lambda}\cos\theta\right)\sin\beta + \left(1 + \frac{r_3}{\lambda}\right)\cos\beta\right)\sin\alpha + \frac{Y_0}{\lambda}$$

$$O_4 = (r_1\sin\theta + r_2\cos\theta)\cos\alpha - ((r_2\sin\theta - r_1\cos\theta)\sin\beta + r_3\cos\beta)\sin\alpha + Y_0$$

$$O_5 = \left(\frac{r_1}{\lambda}\sin\theta + \frac{r_2}{\lambda}\cos\theta\right)\sin\alpha + \left(\left(\frac{r_2}{\lambda}\sin\theta - \frac{r_1}{\lambda}\cos\theta\right)\sin\beta + \left(1 + \frac{r_3}{\lambda}\right)\cos\beta\right)\cos\alpha + \frac{Z_0}{\lambda}$$

$$O_6 = (r_1\sin\theta + r_2\cos\theta)\sin\alpha + ((r_2\sin\theta - r_1\cos\theta)\sin\beta + r_3\cos\beta)\cos\alpha + Z_0$$

4.2.3. *System calibration*

The reconstruction of the actual geometry can be performed through the solution of equations [4.18] and [4.19], which implies the knowledge of several physical parameters, namely X_0, Y_0, Z_0, x, y, α, β, θ, r_1, r_2, r_3, λ and Z. Although, these parameters are possible to measure, their accuracy is determinant for the quality of the system measurements. Therefore, we have developed an automatic calibration method that enables us to calculate these parameters automatically, knowing the exact spatial position of a finite number of points in space and their correspondent localization in the image plane.

Rewriting equations [4.15] and [4.16], we can obtain the following nonlinear equations:

$$x\left(-(X-X_0)\sin\beta+(Y-Y_0)\sin\alpha\cos\beta-(Z-Z_0)\cos\alpha\cos\beta+r_3+\lambda\right)$$
$$-\lambda\left((X-X_0)\cos\beta\cos\theta+(Y-Y_0)(\sin\alpha\sin\beta\cos\theta+\cos\alpha+\sin\theta)\right.$$
$$\left.+(Z-Z_0)(\sin\alpha\sin\theta-\cos\alpha\sin\beta\cos\theta)+r_1\right)=0$$

[4.20]

$$y\left(-(X-X_0)\sin\beta+(Y-Y_0)\sin\alpha\cos\beta-(Z-Z_0)\cos\alpha\cos\beta+r_3+\lambda\right)$$
$$+\lambda\left((X-X_0)\cos\beta\sin\theta-(Y-Y_0)(\cos\alpha\cos\theta-\sin\alpha\sin\beta\sin\theta)\right.$$
$$\left.-(Z-Z_0)(\cos\alpha\sin\beta\sin\theta+\sin\alpha\cos\theta)+r_2\right)=0$$

[4.21]

Analyzing equations [4.15] and [4.16], we recognize that knowing the spatial location of a point (X,Y,Z) and its correspondent image location (x, y), we have as system unknowns, the variables X_0, Y_0, Z_0, α, β, θ, r_1, r_2, r_3 and λ.

Knowing that the maximal number of spatial independent equations that we can generate corresponds to three non-collinear points (six equations) (see [GON 87]), we have to reduce the number of unknowns to six.

The parameters r_1, r_2, r_3 and λ do not change with the camera position as these values are the camera manufacturer's parameters. Therefore, we can fix these parameters through accurate measurements in a laboratory. It follows that the set of unknowns is now reduced to six: X_0, Y_0, Z_0, α, β and θ. These six unknowns are automatically calculated with the knowledge of three non-collinear points in space and their correspondent localization in the image plane.

Newton-Raphson method is the numerical method used to solve the correspondent set of nonlinear equations [4.20] and [4.21] [CON 81].

Figure 4.10 shows the reference image to calibrate the system and the test image to determine the accuracy of the performed calibration.

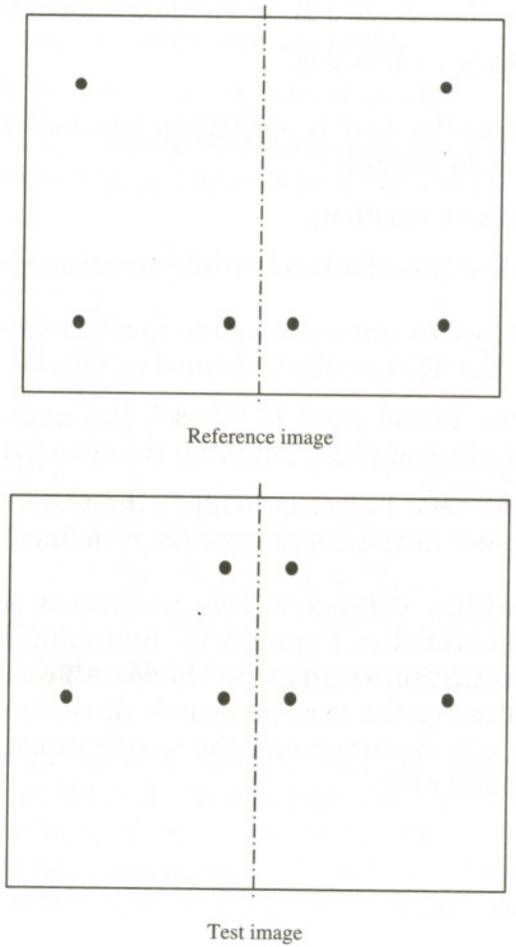

Figure 4.10. *Reference and test images*

4.3. Image processing algorithm

The illumination conditions are of major importance in simplifying a general algorithm for image processing.

In the present case, the illumination conditions were set in a specific way so that the obtained image can be binary processed. Only two levels of pixels were defined:

– white pixels – value > K (predefined parameter);

– black pixels – value < K.

To elaborate the search algorithm, two major additional parameters were defined:

– initial search position;

– search directions for black–white transitions.

The main search criterion for the identification of a pixel belonging to the light profile is defined as follows:

– when the tested pixel is "black", the next pixel to be tested is the adjacent pixel, following the search direction;

– when the tested pixel is "white", the transition pixel is found and a new initial search position is defined.

The algorithm defined above, to process the profile's image, is illustrated in Figure 4.11. Analyzing Figure 4.11, the search algorithm begins with the identification of points 1 and 2, following the vertical search directions n_1 and n_2. Then, point x is identified and the search direction changes to the horizontal axis.

4.4. Results

4.4.1. *Building the wheel's profile in the horizontal light plane*

From the knowledge of the image's dual profile (Figure 4.11), we reconstruct the static wheel's profile according to equation [4.22] as is illustrated in Figure 4.12:

$$y_i = \left(y_{\text{ref}_i} - y_{\text{comp}_i} - \text{CDROL}\right)/2 \qquad [4.22]$$

where:

y_{ref} is coordinate of the forward profile;

y_{comp} is coordinate of the backward profile;

CDROL is circumference's horizontal chord correspondent to the theoretic rolling diameter (see Figures 4.1 and 4.2).

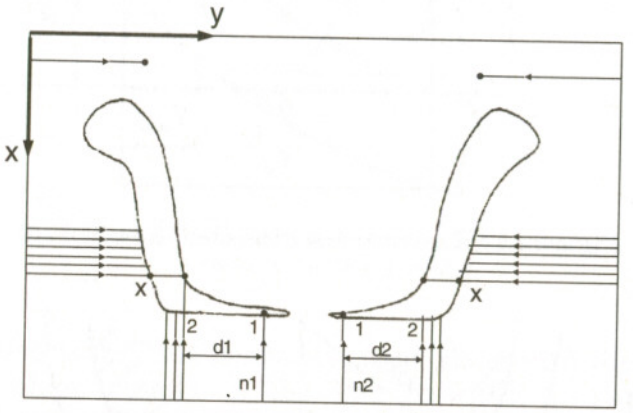

Figure 4.11. *Image processing algorithm*

Knowing the value of CDROL, also previously referred to in equation [4.22] and Figures 4.12 and 4.13, and ALT, the height of the light plane secant to the wheel, illustrated in Figure 4.13, the calculation of the wheel's diameter can be carried out as indicated in Figure 4.13, using equation [4.23].

$$\text{DIAM} = \frac{\text{CDROL}^2 + \text{ALT}^2}{\text{ALT}} \qquad [4.23]$$

where:

DIAM is the wheel's diameter correspondent to the circumference's horizontal chord CDROL;

CDROL is the circumference's horizontal chord correspondent to the theoretic rolling diameter;

ALT is the height of the light plane secant to the wheel.

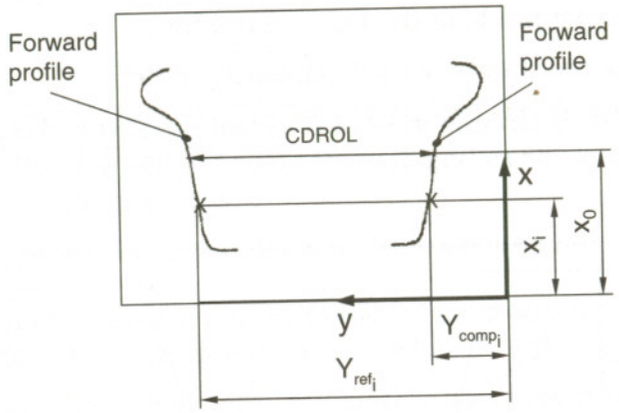

Figure 4.12. *Reconstruction of the static wheel's profile*

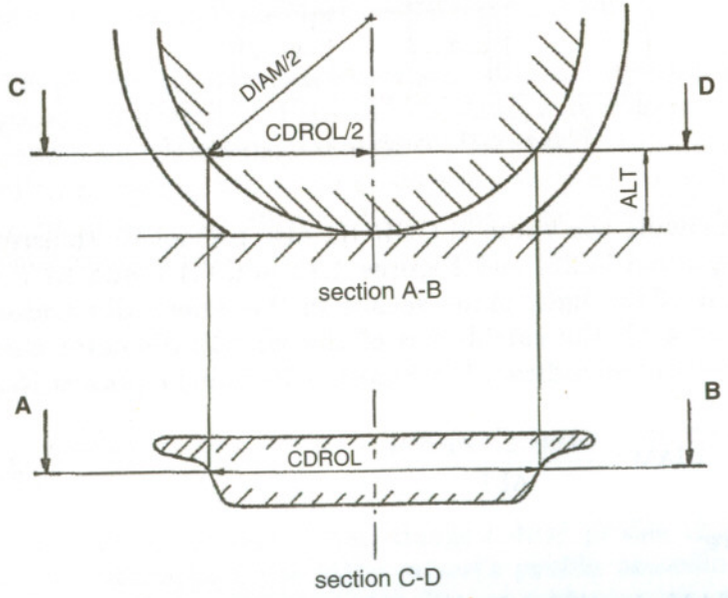

Figure 4.13. *Calculation of the wheel's diameter*

4.4.2. *Building the wheel's profile in the radial plane*

Knowing the wheel's profile in the horizontal light plane, we have to project this profile in the radial plane as shown in Figure 4.14.

Figure 4.14. *Projection of the horizontal wheel's profile in the radial plane*

Intersection of the horizontal light plane with the wheel's radial plane results in the line r, which is parallel to the wheel's axis, as illustrated in Figure 4.15. This line intersects the wheel's radial profile in the theoretical rolling point, P, as indicated in Figure 4.15 and previously referred to in Figures 4.1 and 4.2.

Having defined the theoretical rolling diameter, the wheel's radial profile is divided into two zones, as illustrated in Figure 4.16:

– zone I: diameters smaller than the theoretical rolling diameter;

– zone II: diameters greater than the theoretical rolling diameter.

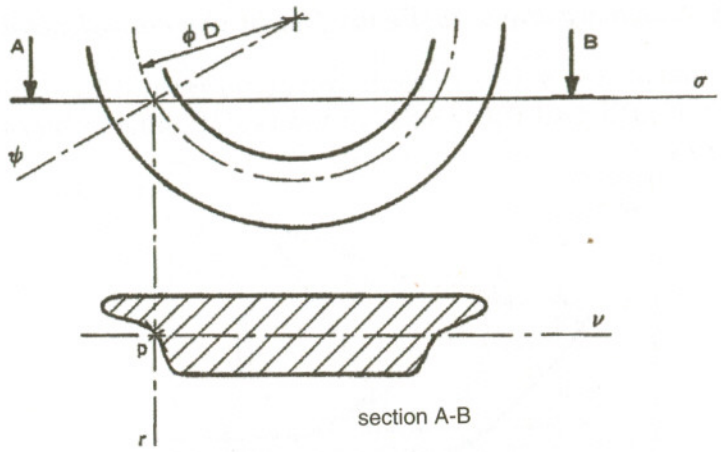

Figure 4.15. *Intersection of the horizontal light profile with the wheel's radial profile (definition of the theoretical rolling point P)*

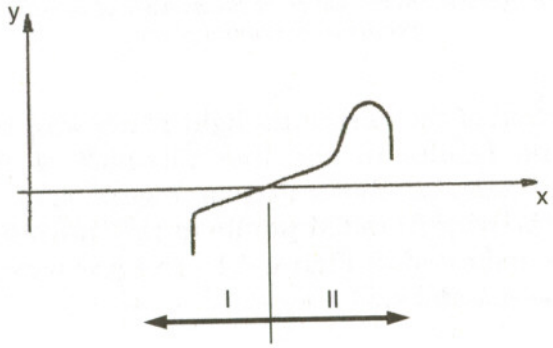

Figure 4.16. *Two main zones of the wheel's radial profile regarding the theoretical rolling diameter*

Finally, the wheel's profile in the axial plane can be built for both the zones I and II, according to the following equations (equations [4.24] and [4.25]) and using Figure 4.17:

$$R_I = -\left(\mathrm{ROL} - \sqrt{(\mathrm{AUX2} - H_I)^2 + \mathrm{AUX1}}\right) \quad [4.24]$$

$$R_{II} = \sqrt{(\mathrm{AUX2} - H_{II})^2 + \mathrm{AUX1}} - \mathrm{ROL} \quad [4.25]$$

where:

$$\mathrm{AUX1} = (\mathrm{ROL} - \mathrm{ALT})^2 \quad [4.26]$$

$$\mathrm{AUX2} = \sqrt{(\mathrm{ROL}^2 - \mathrm{AUX1})} \quad [4.27]$$

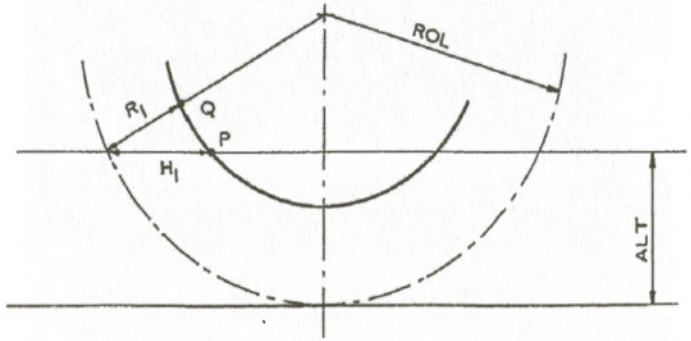

Figure 4.17. *Transformation of the horizontal plane into the radial plane (ex: zone I)*

4.4.3. *Experimental results*

The results shown in this section correspond to the actual measurements performed on a prototype. Figure 4.18 shows the built prototype. The light plane is shown in Figure 4.19.

Figure 4.20 shows the experimental image plane and Figure 4.21 shows the identified dual wheel's profile.

As can be seen from the analysis of Figure 4.20, the light reflection on the wheel's profile causes significant noise in the acquired image. However, this major disturbance being

filtered in the image's processing algorithm and being located in a region where the needed measurements are not affected (see Figure 4.1), it does not influence the quality of the measured data, such as rolling diameter, S_h and S_d, (quantities defined in Figure 4.1).

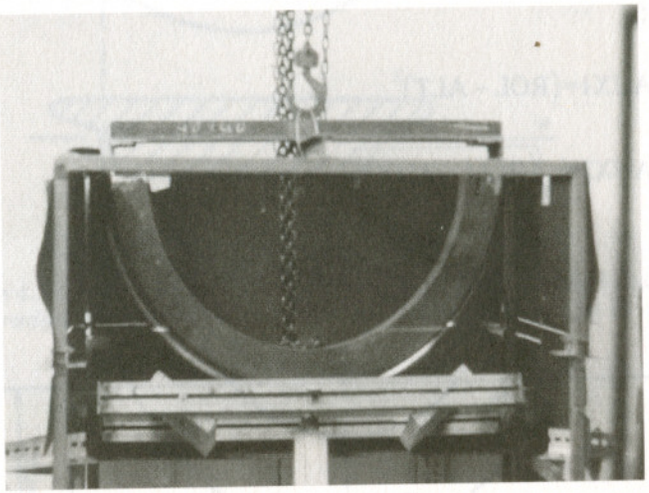

Figure 4.18. *Built prototype*

Figure 4.19. *Intersection of the light plane – wheel*

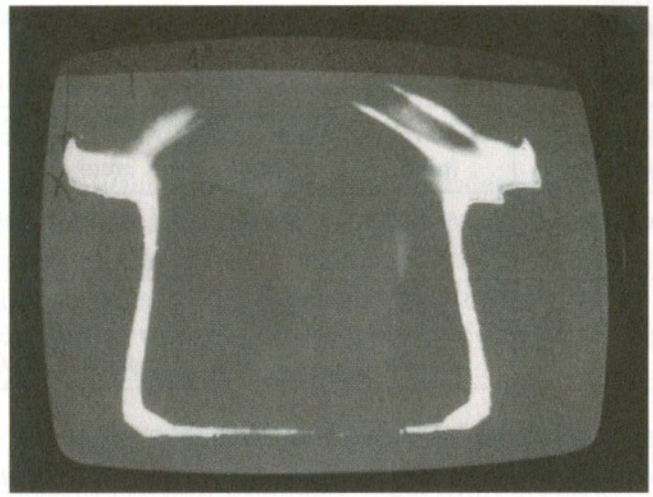

Figure 4.20. *Image plane*

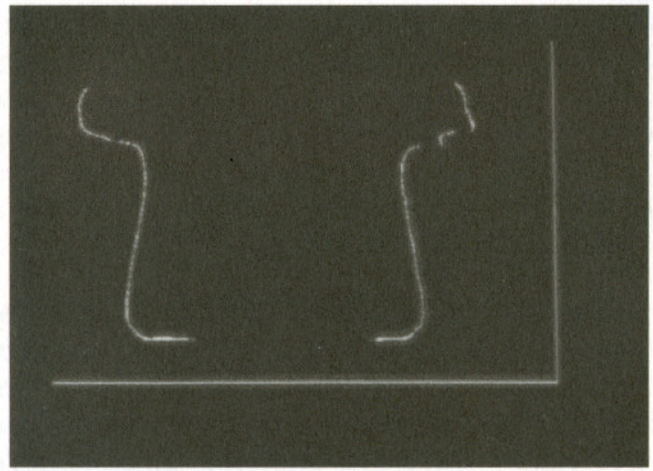

Figure 4.21. *Identified dual wheel's profile*

Table 4.1 shows the results from an experimental measurement made on the prototype, where we were able to reconstruct the reality with a maximal error value that is

less than 0.1 mm. The wheel's measured parameters refer to Figure 4.2.

Dimensional parameters	Actual values [mm]	Meas. values [mm]	Abs. error [mm]	Rel. error [%]
Theor. rolling diameter	860,000	860,073	–0.073	–0.01%
S_h	24,562	24,550	0.012	0.05%
S_d	35,803	35,799	0.004	0.01%

Table 4.1. *Prototype's measurement results*

Finally, Figure 4.22 shows the wheel's radial profile together with the automatic measured data, as shown to the operator.

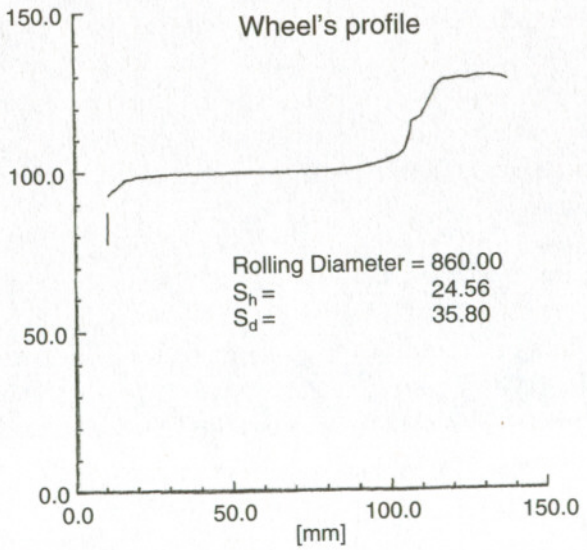

Figure 4.22. *Measured wheel's profile*

4.5. Conclusions

This chapter describes a successful example of cooperation between university and industry.

The case study presented here is related to the field of industrial maintenance, concerning the measuring and monitoring of the railroad wheel profiles in the Portuguese railway company, CP – Comboios Portugal. A vision system to measure the wearing of the wheels of a train moving at a slow speed of 5 km/h is developed.

A static 1:1 scale prototype is developed and the calibration and testing procedures are presented. The developed prototype is based on an image processing system to provide for the automatic measurement of moving railroad wheels. The wheel's profile is acquired by the illumination of the wheel through a secant and horizontal light plane. This profile's image is processed by identifying the line of the greatest light gradient in the whole image. This gradient profile is then converted into the wheel's radial profile by means of a coordinate transformation model, which transforms the image plane into the wheel's radial plane.

The results correspond to actual measurements carried out on a prototype. Significant noise was observed in the acquired image due to the high light reflection on the wheel's profile. However, this major disturbance being filtered in the image's processing algorithm and being located in a region where the needed measurements are not affected, it does not influence the quality of the measured data.

The measurements show very good accuracy, with relative errors below 0.1%.

4.6. Acknowledgment

This work was partially supported by the Strategic Project, PEst-OE/EME/LA0022/2011, through FCT (under the Unit IDMEC – Pole IST, Research Group IDMEC/LAETA/CSI).

4.7. Bibliography

[ALE 98] ALEXANDRE L., CAMPILHO A., A 2D Image Motion Detection Method Using a Stationary Camera, RECPAD98, 1998.

[BRO 10] BROWN R., HANN C., CHASE G., "Vision-based 3D surface motion capture for the DIET breast cancer screening system", *International Journal of Computer Applications in Technology,* vol. 39, no. 1/2/3, pp. 72–78, 2010.

[CHE 12] CHEN H., MA S., SUN B., SHEN Y., "Projection ray intersection location-based multicolour pseudo-random coded projected active vision method", *International Journal of Computer Applications in Technology,* vol. 43, no. 1, pp. 21–28, 2012.

[CON 81] CONTE S., BOOR C., *Elementary Numerical Analysis – An Algorithmic Approach*, 3rd ed., McGraw-Hill, 1981.

[CUI 08] CUI J., ZHA H., ZHAO, H., SHIBASAKI R., "Multi-modal tracking of people using laser scanners and video camera", *Image and Vision Computing,* vol. 26, pp. 240–252, 2008.

[DU 08] DU C., SUN D., "Multi-classification of pizza using computer vision and support vector machine", *Journal of Food Engineering*, vol. 86, pp. 234–242, 2008.

[FAT 95] FATHY M., SIYAL M., "An image detection technique based on morphological edge detection and background differencing for real-time traffic analysis", *Pattern Recognition Letters,* 16, pp. 1321–1330, 1995.

[FIG 08] FIGUEIREDO J., "Measuring railroad wheel profiles through image processing technology", *Proceedings of 18th IASTED International Conference on Visualization, Imaging and Image Processing – VIIP 2008,* Palma de Mallorca, Spain, September 2008.

[GON 87] GONZALEZ R., *Digital Image Processing*, Addison-Wesley Publishing Company, 1987.

[GOU 07] GOUTTIÈRE C., CONINCK J., "Detection of synthetic singularities in digital mammographies using spherical filters", *Proceedings of ECCOMAS Thematic Conference on Computational Vision and Medical Image Processing,* Porto, Portugal, 2007.

[GRI 07] GRILO F., FIGUEIREDO J., DIAS O., AMARAL T., "Adaptive topologies for dimension of cells in 2D-images for movement detection", *Proceedings of the IEEE International Symposium on Intelligent Signal Processing – WISP 2007,* Madrid, Spain, October 2007.

[GRI 08] GRILO F., FIGUEIREDO J., "An industrial vision system for quality control based on a distributed strategy", *Proceedings of International Conference on Automatic Control – CONTROLO 2008,* Vila Real, Portugal, 2008.

[GRI 09] GRILO F., FIGUEIREDO J., DIAS O., AMARAL T., "Adaptive method for skin detection in coloured images", *Proceedings of the IEEE International Conference on Mechatronics*, Malaga, Spain, April 2009.

[HLO 03] HLOU L., LICHIOUI A., GUENNOUN, Z., "Degraded 3D-objects restoration and their envelope extraction", *International Journal of Robotics and Automation,* vol. 18, no. 2, 2003.

[JAI 81] JAIN A., "Image data compression: a review", *Proceedings of IEEE*, vol. 69, no 3, pp. 349–389, 1981.

[JAI 95] JAIN R., KASTURI R., SCHUNK B., *Machine Vision,* McGraw Hill, 1995.

[KIM 10] KIM H., LEE K., KIM S., YANG H., "A precise inspection technique for wafer pre-sawing lines using affine transformation", *International Journal of Computer Applications in Technology,* vol. 39, no.1/2/3, pp. 46–52, 2010.

[LEE 06] LEE J., SHINOZUKA M., "A vision-based system for remote sensing of bridge displacement", *NDT&E International,* vol. 39, pp. 425–431, 2006.

[LIM 11] LIM K., DU T., WANG Q., "Partially occluded object recognition", *International Journal of Computer Applications in Technology,* vol. 40, nos. 1/2, pp. 122–131, 2011.

[MES 10] MESSON C., "Synchronisation of vision-based sensor networks with variable frame rates", *International Journal of Computer Applications in Technology,* vol. 39, nos. 1/2/3, pp. 153–158, 2010.

[MIT 96] MITCHELL J., PENNEBAKER W., FOGG C., LEGALL D., *MPEG Video Compression Standard*, Chapman & Hall, 1996.

[NEL 03] NELSON B., "A distributed framework for visually servoed manipulation using an active camera", *International Journal of Robotics and Automation,* vol. 18, no. 2, 2003.

[PAI 10] PAI Y., LEE L., RUAN S., CHEN Y., MOHANTY S., KOUGIANOS E., "Honeycomb model based skin colour detector for face detection", *International Journal of Computer Applications in Technology*, vol. 39, nos. 1/2/3, pp. 93–100, 2010.

[YAN 10] YANG T., ZHU K., RUAN Q., HAN D., "Moving target tracking and measurement with a binocular vision system", *International Journal of Computer Applications in Technology,* vol. 39, nos. 1/2/3, pp. 145–152, 2010.

[ZHA 10] ZHANG Z., CHEN Z., SHI J., JIA F., DAI M., "Surface roughness vision measurement in different ambient light conditions", *International Journal of Computer Applications in Technology,* vol. 39, nos. 1/2/3, pp. 53–57, 2010.

[ZHA 12] ZHANG X., GONG F., XU L., "Inspection of surface defects in copper strip using multivariate statistical approach and SVM", *International Journal of Computer Applications in Technology,* vol. 43, no. 1, pp. 44–50, 2012.